This article is published in Journal of Thermophysics and Heat Transfer, Vol. 28, No. 2 (2014)
and available at : https://doi.org/10.2514/1.T4190

# Effect of High-enthalpy Air-chemistry on Stagnation Point Heat Flux

D. Siva K. Reddy,* Bijaylakshmi Saikia† and Krishnendu Sinha‡

*Indian Institute of Technology Bombay, Mumbai 400076, India*

## Nomenclature

| | |
|---|---|
| $k_f$ | forward reaction rate coefficient, $m^3/(kg\text{-}mol.s)$ |
| $k_b$ | backward reaction rate coefficient, $m^3/(kg\text{-}mol.s)$ or $m^6/(kg\text{-}mol^2.s)$ |
| $l$ | wall-normal distance, m |
| $q$ | heat transfer rate, $W/cm^2$ |
| $R$ | net reaction rate for a chemical reaction, $kg\text{-}mol/(m^3.s)$ |
| $Y$ | species mass fraction |
| $\delta$ | thermal boundary-layer thickness, m |

## I. Introduction

Re-entry flows are characterized by high-temperature effects, like internal energy excitation, chemical reactions and ionization. The thermo-chemical processes and their non-equilibrium effects determine the temperature of the gas that envelops the vehicle. They also alter the gas composition and associated properties, like conductivity and viscosity of the gas mixture. These have dominant effect on the shock stand-off distance, surface heat flux and other aero-thermodynamic characteristics of the vehicle.

The accuracy of computational fluid dynamic simulations at re-entry conditions depends on the fidelity of the different thermo-chemical models used in the simulation. Several research efforts have been directed in the recent past towards quantifying the sensitivity of the aero-thermal predictions to the uncertainty in the model parameters.[1,2] Flow simulations usually involve a large number of thermo-chemical parameters, like the rate constants of chemical reactions, vibrational-translational relaxation times, and species diffusion

*Doctoral student, Department of Aerospace Engineering. Currently at Mahindra & Mahindra Ltd., Chengalpattu, India.
†Doctoral student, Department of Aerospace Engineering
‡Associate Professor, Department of Aerospace Engineering, Senior AIAA Member.

coefficients. The chemical rate constants form a significant portion of the parameter space for uncertainty analysis.[3] Also, the typical uncertainty in the available reaction rate values (± 1 order of magnitude) is one of the highest among all the model parameters.[4] It is therefore important to study the effect of chemical reaction rates on aero-thermodynamic predictions.

Many different thermo-chemical reactions can occur in a given re-entry flow and there are often competing effects between these processes. A detailed study of the underlying physics is required to identify the dominant mechanisms and their rate-limiting steps. Such insight can help explain flow phenomena observed at high-enthalpy conditions. It can also provide valuable information regarding the sensitivity of aero-thermodynamic predictions to uncertainty in the thermo-chemical parameters.

With in this scope, Reddy and Sinha[5] investigated the effect of chemical reaction rates on convective heat flux prediction at the 35 km altitude trajectory point (1652.75 sec after launch) of the FIRE II capsule. Numerical simulations were performed by varying the reaction rate constants as per their uncertainty limits. The flowfield solutions thus computed were analyzed in terms of the variations in local chemical reaction rates and the species source terms. The resultant effect on the gas composition and temperature in critical regions of the flowfield, like the thermal boundary layer on the surface, was studied. It was found that the chemical state of the gas, i.e., equilibrium, nonequilibrium or frozen, and the extent of recombination reactions in the boundary layer are the critical factors that determine the sensitivity of the heating rate to variations in the reaction rate coefficients.

In the current paper, we apply a similar approach to a high-enthalpy AS-202 re-entry condition, which has been numerically simulated by Wright *et al.*[6] The Mach number is 26.2 and the total enthalpy is 31.53 MJ/kg. The dominant chemical activity observed at the 35 km altitude condition (total enthalpy of 12 MJ/kg) is the dissociation and recombination of oxygen. The surface heating rate is therefore sensitive to only these reaction rates. A higher total enthalpy at the 70 km condition can cause dissociation and recombination of both $O_2$ and $N_2$, and multiple reactions are expected to proceed simultaneously. We aim to investigate the sensitivity of the flowfield solution to variation in these reaction rates, and to identify the critical parameters that influence the accuracy of the surface heat flux predictions. The focus of the current work is on gas-phase chemistry, and therefore wall catalysis effects are not included.

## II. Simulation Methodology

The simulation methodology used here is identical to that in Ref. 5 and the key points are highlighted. The freestream density, velocity and temperature for the chosen condition are 0.000152 kg/m$^3$, 7920 m/s and 227 K, respectively. The chemically reacting hypersonic flow at this condition is simulated by solving the Navier-Stokes equations along with species conservation equations and the two-temperature thermal non-

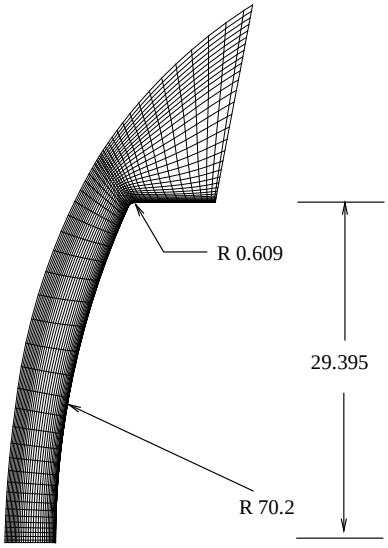


Figure 1: Capsule geometry and a typical computational grid used in the simulation. The dimensions are marked in cm and every second point in the wall-parallel and wall-normal directions are shown.

equilibrium model of Park.[7] Air is modeled as a neutral mixture of five perfect species ($N_2$, $O_2$, NO, N and O) with three dissociation and two exchange reactions.

$$N_2 + M \rightleftharpoons 2N + M \tag{1}$$

$$O_2 + M \rightleftharpoons 2O + M \tag{2}$$

$$NO + M \rightleftharpoons N + O + M \tag{3}$$

$$N_2 + O \rightleftharpoons NO + N \tag{4}$$

$$NO + O \rightleftharpoons O_2 + N \tag{5}$$

where M is the collision partner. The five reactions are referred to as per the above numbers and their rates are denoted by $R_i$ for $i = 1, \ldots, 5$. The baseline forward and backward rate constants are evaluated from the curve fits given in Ref. 7. The data shows that the uncertainty in the measurement of chemical rate constants is about one order of magnitude. Simulations are thus performed by increasing and decreasing the chemical reaction rate constants by a factor of ten as compared to the baseline values. This is achieved by multiplying both $k_f$ and $k_b$ by a reaction scaling factor (rsf). A value of rsf = 10 corresponds to higher reactivity simulation, rsf = 0.1 represents lower reactivity case, and rsf = 1 is baseline simulation. The procedure is identical to that described in Ref. 5.

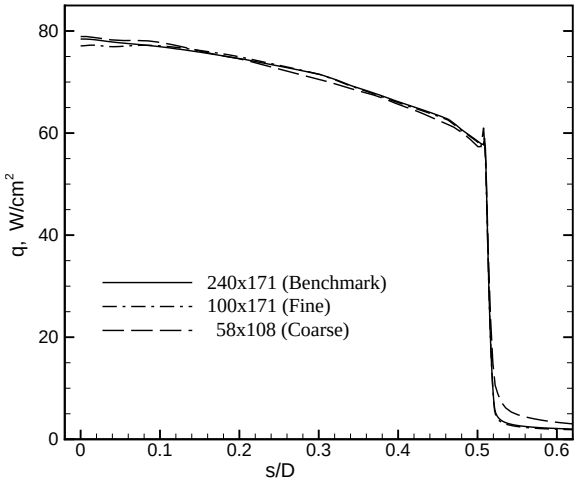


Figure 2: Effect of grid refinement on forebody surface heat flux.

The axisymmetric form of the governing equations is discretized using the finite-volume method. Inviscid fluxes are computed using a modified (low-dissipation) form of the Steger-Warming flux splitting approach.[8] The method is second-order accurate in both streamwise and wall-normal directions. The viscous fluxes are evaluated using second-order accurate central differencing, and the implicit data parallel line relaxation method[9] is used to obtain steady-state solution. The code has been validated against flight data for re-entry conditions.[10] No-slip, non-catalytic and isothermal boundary conditions are specified at the wall. Both vibrational and translational temperatures are set to 553.3 K at the wall, and is same as that used earlier.[5] The forebody geometry (see Fig. 1) is also identical to that used in the previous study.[5] Since the freestream Reynolds number based on body diameter is 4.79 $\times 10^4$, laminar simulations are performed.

A typical grid used in the simulation is shown in Fig. 1. The grid in the wall-parallel direction is designed such that points are clustered in the nose stagnation region and at the shoulder expansion corner. The wall-normal grid is refined both in the vicinity of the shock wave as well as in the near-wall region. Note that the solution is highly sensitive to mis-alignment of the grid lines to the shock shape. We use the algorithm proposed by Saunders *et al.*[11] to carefully tailor the grid lines to the bow shock and eliminate numerical irregularities in the predicted surface heat flux.

Figure 2 shows the wall heating rates computed using three successively refined meshes – coarse (58×108), fine (100×171) and benchmark (240×171). All the grids are obtained after multiple iterations of the shock-alignment procedure. The forebody heating rates obtained on the fine and benchmark grids are identical, except for small deviations in the stagnation region. The coarse mesh predictions also compare well with the other solutions and they are within 1% of the benchmark solution in the stagnation region. The 58×108 mesh is chosen for further analysis, due to its robustness to the grid-shock mis-alignment. The wall-normal spacing is $1\times10^{-6}$ m and the corresponding cell Reynolds number is 0.83 or less. Further details of the grid

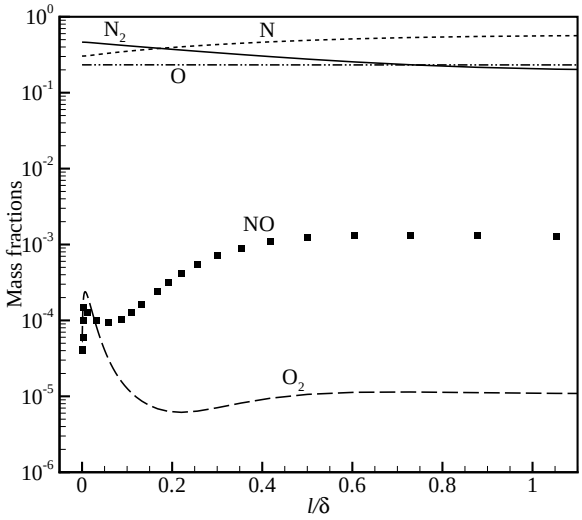


Figure 3: Variation of species mass fraction in the thermal boundary layer at the nose stagnation point.

convergence study and the grid-alignment procedure can be found in Ref. 12.

## III. Results

The variation of the gas composition in the thermal boundary layer at the nose stagnation point is presented in Fig. 3. Oxygen is almost completely dissociated and nitrogen is partially dissociated behind the bow shock. The corresponding mass fractions at the boundary layer edge ($l/\delta = 1$) can be noted in the figure. The gas is in thermal equilibrium at the boundary-layer edge, with translational and vibrational temperatures around 6560 K. In the boundary layer, both temperatures decrease monotonically to reach the cold-wall value and the mass fraction of $N_2$ increases, with a corresponding decrease in $Y_N$. However, $Y_O$, $Y_{O_2}$ and $Y_{NO}$ remain almost constant throughout the boundary layer.

Figure 4 shows that the chemical reactions are effective in the vicinity of the wall ($l/\delta < 0.05$). The largest reaction rate corresponds to the NO recombination reaction (3). The NO molecules thus created collide with the available N atoms to form $N_2$ molecules through the exchange reaction (4). For $l/\delta > 0.005$, it is seen that $R_3 \simeq R_4$, and the net effect of the two reactions is $2N \rightarrow N_2$.

Availability of NO molecules is critical for continuation of the exchange reaction (4). As $R_3$ drops to negligible values for $l/\delta < 0.004$, the magnitude of $R_4$ decreases. The rates $R_2$ and $R_5$ increase in this near-wall region and provide the NO required for reaction (4). The resulting reaction mechanism that leads to the conversion of N atoms to $N_2$ molecules is as follows. First, the recombination of oxygen atoms occurs via backward reaction (2). The oxygen molecules thus formed collide with N atoms, as per reaction (5), resulting in the formation of NO and O atoms. The newly created NO molecules further react with the available N

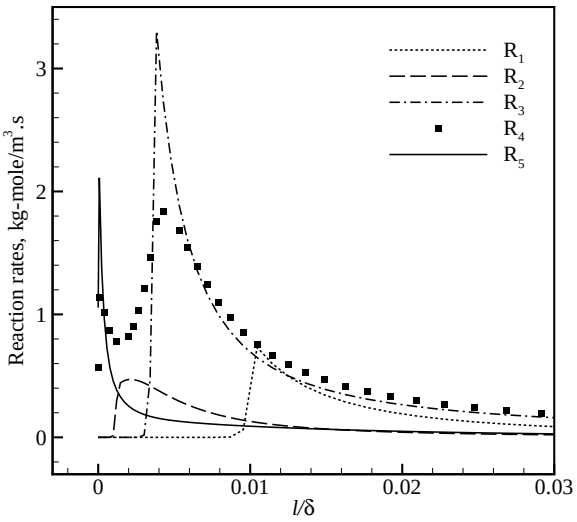


Figure 4: Variation of chemical reaction rates in the thermal boundary layer at the nose stagnation point.

atoms to form $N_2$ molecules via reaction (4). Thus, $O_2$ molecules act as a catalyst for $N_2$ recombination.

The conversion of N atoms to $N_2$ molecules in the boundary layer thus occurs via two competing reaction mechanisms. The NO mechanism comprises of reactions (3) and (4), and is initiated by NO recombination. The $O_2$ mechanism, consisting of reactions (2), (4) and (5), is initiated by $O_2$ molecules. The majority of $N_2$ recombination at the current condition occurs via the first mechanism, because the rate coefficient of NO recombination is higher than that of $O_2$ recombination.

## A. Altered reactivity in the boundary layer

Numerical simulations are performed by changing the rate constants of the five reactions, either individually or simultaneously. The reaction rate constants are altered only in the boundary layer to study their local effect. Solutions obtained by changing the reaction rates in the entire domain are analyzed in Ref. 12.

NO recombination is a key step for $N_2$ formation in the baseline simulation. Enhancing the corresponding rate constant, by setting rsf = 10, increases $N_2$ formation in the boundary layer, and the reverse is true for rsf = 0.1; the values are reported in Table 1. Setting rsf = 10 for $O_2$ recombination also enhances $N_2$ concentration in the boundary layer. Suppressing $O_2$ recombination (rsf = 0.1) has a small effect, because the $O_2$ mechanism has a minimal contribution towards $N_2$ formation in the baseline simulation. Altering the rate constants of exchange reactions (4) and (5), both rsf = 10 and 0.1, has negligible effect. Thus, we can say that $O_2$ and NO recombination reactions are the rate-limiting steps in the $N_2$ recombination process.

Next, we increase the rate constants of all five chemical reactions simultaneously in the boundary layer. The rates $R_2$, $R_4$ and $R_5$ are enhanced significantly, such that the $O_2$ mechanism is preferred in this case, as compared to the dominant NO mechanism in the baseline simulation. An increase in the rate constant of $O_2$

Table 1: Stagnation point heating rate (in W/cm$^2$) and mass fractions of $O_2$ and $N_2$ at the wall obtained when the chemical rate constants are altered in the boundary layer. Percentage changes in $Y_{N_2}$ and $q$ with respect to the baseline simulation (rsf = 1) are reported.

| Reaction | rsf | $Y_{O_2}$ | $Y_{N_2}$ | $\Delta Y_{N_2}$ (%) | $q$ | $\Delta q$ (%) |
|---|---|---|---|---|---|---|
| Baseline | 1.0 | $5.03\times10^{-5}$ | 0.44 | – | 78.91 | – |
| $NO + M \rightleftharpoons N + O + M$ | 10.0 | $1.69\times10^{-4}$ | 0.65 | 47.73 | 116.49 | 47.62 |
| $O_2 + M \rightleftharpoons 2O + M$ | 10.0 | $8.96\times10^{-4}$ | 0.54 | 22.73 | 101.56 | 28.70 |
| $N_2 + O \rightleftharpoons NO + N$ | 10.0 | $4.99\times10^{-5}$ | 0.43 | -2.27 | 80.48 | 1.98 |
| $NO + O \rightleftharpoons O_2 + N$ | 10.0 | $5.26\times10^{-7}$ | 0.44 | 0.00 | 79.55 | 0.81 |
| $N_2 + M \rightleftharpoons 2N + M$ | 10.0 | $8.36\times10^{-5}$ | 0.54 | 22.73 | 94.42 | 19.66 |
| All five reactions | 10.0 | $1.40\times10^{-4}$ | 0.68 | 54.55 | 126.33 | 60.09 |
| $NO + M \rightleftharpoons N + O + M$ | 0.1 | $2.79\times10^{-5}$ | 0.35 | -20.45 | 64.28 | -18.54 |
| $O_2 + M \rightleftharpoons 2O + M$ | 0.1 | $4.62\times10^{-6}$ | 0.42 | -4.55 | 78.23 | -0.86 |
| $N_2 + O \rightleftharpoons NO + N$ | 0.1 | $5.00\times10^{-5}$ | 0.44 | 0.00 | 79.62 | 0.90 |
| $NO + O \rightleftharpoons O_2 + N$ | 0.1 | $8.00\times10^{-4}$ | 0.44 | 0.00 | 79.49 | 0.74 |
| $N_2 + M \rightleftharpoons 2N + M$ | 0.1 | $4.39\times10^{-5}$ | 0.41 | -6.82 | 76.71 | -2.79 |
| All five reactions | 0.1 | $4.88\times10^{-5}$ | 0.26 | -40.91 | 46.08 | -41.60 |

recombination reaction results in a higher availability of $O_2$ molecules. This, along with an increased rate constant $k_{b_5}$, enhances the magnitude of $R_5$ more than ten times its baseline value. A higher $R_5$ increases the production of NO and O, which in turn leads to an increase in the magnitude of $R_4$. This results in higher level of $N_2$ and O. The newly created O atoms again recombine to form $O_2$ molecules, which accelerate the $R_2$-$R_5$-$R_4$ loop further. Thus, the $O_2$ mechanism for $N_2$ recombination is a chain mechanism and an increase in one reaction rate recursively enhances the other dependent reactions. The net effect is a large increase in the $N_2$-level in the boundary layer, with a mass fraction of 0.68 at the wall.

The chain reactions $R_2$-$R_5$-$R_4$ will cease when $N_2$ formation is complete. In the absence of N atoms, backward reactions (4) and (5) will be inhibited. Only recombination of oxygen is expected to occur and a build up of $Y_{O_2}$ will be observed. For all the cases listed in Table 1, N atoms are not completely depleted, and therefore no noticeable build up in the mass fraction of $O_2$ in the boundary layer is observed. $Y_{O_2}$ remains in the range of $10^{-4} - 10^{-7}$, which is much smaller than the mass fraction of the dominant species in the gas mixture.

## B. Effect on surface heat flux

The stagnation point heat flux for the baseline and altered reactivity cases are listed in Table 1. The magnitude of heat flux variation in each case correlates directly to the extent of $N_2$ formation in the boundary layer. $Y_{N_2}$ is highest when rsf =10 for all five reactions. Higher recombination increases heat release, which elevates the gas temperature in the near-wall region and results in a higher convective heat transfer to the vehicle wall. All chemical reactions proceed in the exothermic direction in the boundary layer. Altering

the rates of all reactions simultaneously therefore leads to the largest heat flux variation. On similar lines, reducing the rate constants lead to lower heating rates compared to the baseline case. The only exceptions are rsf = 0.1 for reactions (4) and (5), for which the deviations are within the variation due to grid-alignment reported in section II.

The surface heat flux is also a function of the gas conductivity in the near-wall region. At the current boundary-layer conditions, the relative magnitude of thermal conductivity among the species is:

$$\kappa_{\mathrm{N}} > \kappa_{\mathrm{O_2}} > \kappa_{\mathrm{NO}} > \kappa_{\mathrm{N_2}} > \kappa_{\mathrm{O}} \tag{6}$$

Molecular nitrogen has lower thermal conductivity than its atomic counterpart. Increasing (decreasing) the reaction rates results in a higher (lower) mass fraction of $N_2$, thereby reducing (enhancing) the overall mixture conductivity. The changes in conductivity are opposite to those in the near-wall gas temperature mentioned above. The heat release or the temperature effect is found to be the dominant contribution to the surface heat transfer rate. The net effect is an enhancement in the stagnation point heating rate when the rate constants are increased, and a reduction in the heat flux when the rate constants are decreased.

The equilibrium gas composition for the prescribed wall temperature and the computed wall pressure in the baseline simulation is $Y_{\mathrm{N_2}} = 0.767$ and $Y_{\mathrm{O_2}} = 0.233$. The solution computed using the baseline rate constants is far from this equilibrium state. By comparison, in the lower altitude condition studied earlier,[5] the gas density is significantly higher and the gas composition at the wall is close to its local equilibrium level (see Fig. 8b in Ref. 5). Recombination is mostly complete in the baseline simulation at 35 km altitude, and increasing the reaction rates further has minimal effect on the surface heat flux (see Fig. 10 in Ref. 5). On the other hand, a lower gas density at the current 70 km altitude results in a higher degree of non-equilibrium in the flow. The sensitivity of the heat flux predictions to the uncertainty in chemical reaction rates is correspondingly higher than those observed at lower altitude simulations.

## C. Implications for sensitivity analysis

The data presented in Table 1 shows that the surface heat flux is most sensitive to the NO and $O_2$ recombination rates, which are the rate-limiting steps in the $N_2$-recombination mechanisms. The heating rate is also sensitive to the rate of three-body recombination of N atoms. The variation in heating rate due to the uncertainty in other reaction rates is less than 2%. Thus, the backward reaction rate constants $k_{b1}$, $k_{b2}$ and $k_{b3}$, along with three possible collision partners (N, $N_2$ and O), result in nine critical reaction rate parameters in the boundary layer. A full sensitivity analysis will vary the rates of all 17 chemical reactions, which include three dissociation reactions (with five collision partners each) and two exchange reactions. Each reaction has a forward and backward rate constant, adding up to 34 reaction rate parameters. Thus, *a*

*priori* knowledge of the critical parameters can significantly decrease the dimension of the parameter space: from 34 to 9 in this case. Further reduction can be achieved by noting that suppressing $O_2$ recombination has negligible effect on the surface heat flux.

# IV. Conclusions

A re-entry flowfield at Mach 26.2 and 70 km altitude condition is numerically simulated, and the thermochemistry is analyzed along the stagnation stream line. Two competing reaction mechanisms are identified in the boundary layer that convert N atoms to $N_2$ molecules, with no noticeable change in the mass fractions of O, $O_2$ and NO. The first mechanism involves NO recombination, and the second one is initiated by $O_2$ recombination. We study the sensitivity of surface heat flux predictions to changes in the reaction rate constants in the boundary layer. The majority of the heat flux variation is due to uncertainties in the NO and $O_2$ recombination rates, which are the rate-limiting steps for $N_2$ formation. The heating rate values are directly correlated to the extent of $N_2$ recombination in the boundary layer.

# References


[1] Bose, D., Brown, J.L., Prabhu, D.K., Gnoffo, P., Johnston, C.O., and Hollis, B., "Uncertainty Assessment of Hypersonic Aerothermodynamics Prediction Capability," *Journal of Spacecraft and Rockets*, Vol. 50, No. 1, 2013, pp. 12-18.

[2] Sorensen, C., Valentini, P. and Schwartzentruber, T.E., "Uncertainty Analysis of Reaction Rates in a Finite Rate Surface Catalysis Model," AIAA paper 2011-3643, $42^{nd}$ AIAA Thermophysics conference, Honolulu, 2011.

[3] Palmer, G.E., "Uncertainty Analysis of CEV LEO and Lunar Return Entries," AIAA Paper 2007-4253, $39^{th}$ AIAA Thermophysics conference, Miami, 2007.

[4] Bose, D., and Wright, M.J., "Uncertainty Analysis of Laminar Aeroheating Predictions for Mars Entries," AIAA Paper 2005-4682, $38^{th}$ AIAA Thermophysics conference, Toronto, 2005.

[5] Reddy, D.S.K., and Sinha, K., "Effect of Chemical Reaction Rates on Aero-heating Predictions of Re-entry Flows," *Journal of Thermophysics and Heat Transfer*, Vol. 25, No. 1, 2011, pp. 21-33.

[6] Wright, M.J., Prabhu, D.K., and Martinez, E.R., "Analysis of Apollo Command Module Afterbody Heating Part I: AS-202," *Journal of Thermophysics and Heat Transfer*, Vol. 20, No. 1, 2006, pp. 16-30.

[7] Park, C., *Non-Equilibrium Hypersonic Aerothermodynamics*, A Wiley-Interscience Publication, New York, 1990, pp. 35, 255-268 and 326.

[8] MacCormack, R.W., and Candler, G.V., "The Solution of the Navier-Stokes Equations Using Gauss-Siedel Line Relaxation," *Computers and Fluids*, Vol. 17, No. 1, 1989, pp. 135-150.

[9] Wright, M.J., Candler, G.V., and Bose, D., "Data-Parallel Line Relaxation Method for the Navier-Stokes Equations," *AIAA Journal*, Vol. 36, No. 9, 1998, pp. 1603-1609.

[10] Reddy, D.S.K., and Sinha, K., "Hypersonic Turbulent Flow Simulation of FIRE II Reentry Vehicle Afrerbody," *Journal of Spacecraft and Rockets*, Vol. 46, No. 4, 2009, pp. 745-757.

[11] Saunders, D., Yoon, S., and Wright, M., "An Approach to Shock Envelope Grid Tailoring and Its Effect on Reentry Vehicle Solutions ," AIAA Paper 2007-207, 2007.

[12] Reddy, D.S.K., and Sinha, K., "Analysis of High-enthalpy Air-chemistry and its Effect on Stagnation Point Heat Flux," AIAA paper 2012-3002, 43rd AIAA Thermophysics Conference, New Orleans, 2012.